Characteristics of iron-containing magnetic particles in household dust from an urban area: A case study in the megacity of Shanghai

Yinglu Chen, Weiguo Zhang, Chenyin Dong, Simon M. Hutchinson, Huan Feng

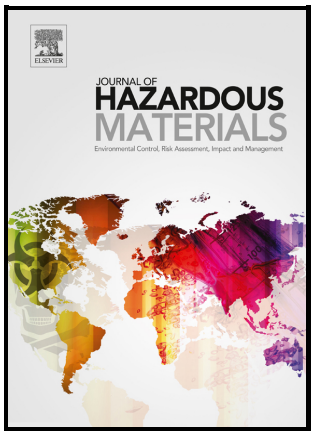

PII: S0304-3894(21)02180-4

DOI: https://doi.org/10.1016/j.jhazmat.2021.127212

Reference: HAZMAT127212

To appear in: *Journal of Hazardous Materials*

Received date: 29 March 2021
Revised date: 7 September 2021
Accepted date: 9 September 2021

Please cite this article as: Yinglu Chen, Weiguo Zhang, Chenyin Dong, Simon M. Hutchinson and Huan Feng, Characteristics of iron-containing magnetic particles in household dust from an urban area: A case study in the megacity of Shanghai, *Journal of Hazardous Materials,* (2021) doi:https://doi.org/10.1016/j.jhazmat.2021.127212

Characteristics of iron-containing magnetic particles in household dust from an urban area: A case study in the megacity of Shanghai

Yinglu Chen[1], Weiguo Zhang[1], Chenyin Dong[2,3]*, Simon M. Hutchinson [4], Huan Feng[5]

[1] State Key Laboratory of Estuarine and Coastal Research, East China Normal University, Shanghai 201100, PR China.

[2] State Environmental Protection Key Laboratory of Environmental Pollution Health Risk Assessment, South China Institute of Environmental Sciences, Ministry of Ecology and Environment, Guangzhou 510655, PR China.

[3] Ministry of Education-Shanghai Key Laboratory of Children's Environmental Health, Xinhua Hospital, Shanghai Jiao Tong University School of Medicine, Shanghai 200092, PR China.

[4] School of Science, Engineering and Environment, University of Salford, Gt. Manchester M5 4WT, UK

[5] Department of Earth and Environmental Studies, Montclair State University, Montclair NJ 07043, USA

***Correspondence to**: dongchenyin@scies.org (C. Dong).

Abstract

In order to characterize the magnetic properties and trace sources of household dust particles, magnetic measurements, geochemical and SEM/TEM analyses were performed on vacuum dust from 40 homes in Shanghai, China. Iron-containing magnetic particles (IMPs) in the household dust were dominated by magnetite, while maghemite, hematite and metallic iron were also present. The IMPs were mainly composed of coarse-grained particles (e.g., >0.1 μm). Ultrafine superparamagnetic (SP) grains (<30 nm) increased proportionately with the abundance of the total IMPs. Household dust had more and coarser IMPs than background soil, but less and finer IMPs than street dust and industrial emissions (coal combustion and

metallurgy). Metallic Fe and spherical IMPs, originating from brake wear abrasion and coal combustion, respectively, have been observed using the SEM/TEM. Contents of magnetic particles were positively correlated to Mo, Ni and Sb, while HIRM was associated with As, Mo, Pb and Sb. The multiple lines of evidence including magnetic measurements, geochemical and SEM/TEM analyses suggested that industrial and traffic emissions and street dust were dominant contributors to the IMPs. Such an approach can help to establish more precisely the sources of household dust particles and could be applied to other indoor contexts and further urban environments.

Keywords:

Magnetic minerals; Indoor environment; Source identification; Industrial activity; Traffic emission

1 **Introduction**

Iron-containing magnetic particles (IMPs), such as metallic iron, magnetite and hematite, are widespread in the environment. They may derive from both natural processes (e.g., rock weathering and erosion processes) and human activities (e.g., coal combustion, traffic emissions) (Snowball et al., 2014; Hofman et al., 2017; Zhang et al., 2020). Anthropogenic IMPs have been observed widely, including those originating from metallurgy, vehicle exhaust emissions, vehicle brake and tire wear and emissions from coal combustion (Gonet and Maher, 2019). For example, IMPs generated at rail-wheel-brake and the overhead catenary–pantograph interfaces are enriched in subway airborne particulate levels especially at underground stations (e.g., Zhang et al., 2011; Jung et al., 2012; Moreno et al., 2015; Cui et al., 2016). Spherical IMPs, typically produced by coal combustion, are found in fluvial sediments, street dust and urban surface soil (Petrovsky and Ellwood, 1999; Mitchell and Maher, 2009; Wang et al., 2018, 2019). Magnetic measurements that examine the abundance of IMPs, their particle size and mineralogy have been widely used to reflect heavy metal contamination and trace particle sources as a rapid, economic and non-destructive approach (e.g., Maher and Thompson, 1999; Zhang et al., 2011; Chaparro et al., 2017; Ge et al., 2017; Hatfield et al., 2019; Wang et al., 2018, 2019; Wang et al., 2020; Li et al., 2021). In recent

years, the exposure risk of IMPs themselves, especially for nano-sized particles (<100 nm) has drawn public concerns (Maher et al., 2016; Calderón-Garcidueñas et al. 2019; Lu et al., 2020; Liu et al., 2021).

In terms of the potential adverse effects of IMPs on human health, studies examining the mineralogy, abundance and sources of IMPs in atmospheric particulate matter have recently been conducted (e.g., Zhang et al., 2020; Pattammattel et al., 2021). However, the occurrence and characteristics of IMPs, especially nano-sized iron-containing magnetic particles (NIMPs) in domestic indoor environments, are hitherto poorly understood. There are numerous studies showing that the indoor environment can be important in terms of exposure to environmental contaminants (e.g., Turner, 2011; Zhao et al., 2021). The potential health effects associated with household indoor IMPs, especially for those nano-sized particles, cannot be ignored.

Shanghai is one of the most developed and densely populated cities in China. According to statistics in 2018, vehicle ownership in Shanghai reached 4 million (Shanghai Municipal Bureau of Statistics, 2019). The city's coal consumption was approximately 33 million tonnes in 2018 and accounted for approximately 29% of the city's total energy consumption (Shanghai Municipal Bureau of Statistics, 2019). Meanwhile, there were about 5 million people over 60 years old (34% of the total population) in Shanghai in 2018 (Shanghai Municipal Bureau of Statistics, 2019) and therefore more vulnerable to the neurodegenerative and cardiovascular diseases that are potentially linked to IMPs exposure. Household dust is effectively a reservoir of indoor contaminants and has been widely used to study exposure risk of contaminants in the indoor environment (e.g., Ao et al., 2017; Bu et al., 2020; Zhao et al., 2020). In Shanghai, studies have characterized the organic/inorganic pollutant composition of household dust (e.g., organophosphorus flame retardants, PAHs and metals) (Peng et al., 2012; Li et al., 2019). Magnetic measurements have been successfully used to examine the concentration, mineralogy, and grain size of IMPs deriving from traffic and industrial emission sources (e.g., coal combustion, metallurgical manufacturing) in various environmental samples in Shanghai, including atmospheric particles (Shu et al., 2000, 2001), street dust (Yang et al., 2016; Wang et al., 2019), top soil (e.g., Jaffar et al., 2017; Wang et al., 2018) and subway dust (Zhang et al., 2011). However, the characteristics of IMPs in

household dust in Shanghai remain unknown. In this study, we have applied magnetic methods in combination of geochemical and SEM/TEM analyses with the aim to provide a detailed magnetic characterization of Shanghai's household dust. By comparing studies of indoor dust elsewhere in the world, other environmental samples (e.g., surface soil and street dust) in Shanghai, we discuss the concentration, mineralogy and magnetic grain size of IMPs and their sources. Finally, specific attention has been paid to the identification of ultrafine magnetite by the SEM/TEM, due to the considerable health risks associated with the nano-sized fraction of IMPs.

1. Samples and Methods

Non-smoking homes were invited to participate the vacuum dust sampling campaign in this study. Indoor floor dust samples were collected from untouched areas in the living rooms of 40 randomly recruited homes in Shanghai using a vacuum with an high-efficiency particulate absorbing filter between October 2019 and January 2020 (Fig. 1). Detailed information about samples is summarized in Table S1. In the laboratory, the dust samples were sieved to < 250 μm before analysis (U.S. EPA, 2000). Low- and high-frequency magnetic susceptibility (χ: χ_{lf} 0.47 kHz; χ_{hf} 4.7 kHz) was measured using a Bartington Instruments Ltd. MS2 magnetic susceptibility meter. An anhysteretic remanent magnetization (ARM) was acquired in a 0.04 mT direct current field, which was super-imposed on an peak alternating field (AF) of 100 mT and expressed as susceptibility of ARM (χ_{ARM}). Isothermal remanent magnetization (IRM) was imparted in a forward field of 1T and one reversed field (-300 mT) sequentially using an MMPM10 pulse magnetizer. The remanences were measured with an AGICO Dual Speed Spinner Magnetometer (JR6). The IRM imparted with a 1T field is referred to as saturation IRM (SIRM). The S ratios (S_{-300}) is calculated as $S_{-300}=100\times(SIRM-IRM_{-300mT})/(2\times SIRM)$ (Bloemendal et al., 1992). Hard isothermal remanent magnetization (HIRM) is calculated as $HIRM=(SIRM+IRM_{-300mT})/2$ (Bloemendal et al., 1988). The frequency dependent susceptibility was calculated as $\chi_{fd}\%=100\times(\chi_{lf}-\chi_{hf})/\chi_{lf}$ (Maher, 1986).

INSERT FIGURE 1

Selected samples were subject to thermomagnetic analysis using a Variable Field Translation Balance (VFTB) with a heating temperature up to 800°C. The magnetization field was set at 36 mT. Magnetic hysteresis, IRM acquisition curve and first-order reversal curve (FORC) were measured using a Lakeshore 8604 Vibrating Sample Magnetometer (VSM). IRM acquisition curves were acquired in 60 fields ranging from 10 mT to 1 T. The field intervals were approximately equidistant on a log scale. IRM acquisition curves were unmixed using the fitting protocol of Kruiver et al., (2001). For FORC measurements, the maximum applied field is 500 mT with field increments up to 1.57 mT resulting in a total of 140 FORCs. FORC diagrams were calculated using FORCinel software v3.06 (Harrison and Feinberg, 2008). These samples were processed with the VARIFORC smoothing parameters $S_{c,0}$=8, $S_{c,1}$=10, $S_{b,0}$=7, $S_{b,1}$=10, and $\lambda_c=\lambda_b$=0.1 (Egli, 2013). To reflect the proportion of SP grains, normalized ferrimagnetic susceptibility is calculated as $\chi_f/Ms=(\chi-\chi_p)/Ms$ (Hunt et al., 1995), where χ_f represents the purely ferrimagnetic susceptibility, χ_p represents paramagnetic susceptibility and is obtained from the high-field slope of the hysteresis curves (Hunt et al., 1995) and Ms represents saturation magnetization.

To identify the morphology and composition of magnetic particles in the dust, magnetic particles were extracted from bulk samples by adapting the methods of Petersen et al., (1986). Dust sample (~0.2g) was dispersed in Milli-Q water and ultrasonized for 30 minutes (Zhang et al., 2020), then a rare-earth magnet wrapped in a plastic film was used to extract IMPs. The extracted IMPs were washed into an evaporating dish and dried at the room temperature before further analysis. Extracted magnetic particles were analyzed using a TALOS F200X transmission electron microscope (TEM) and a MIRA3 scanning electron microscope (SEM) with an energy dispersive X-ray analyzer (EDS).

About 0.5g of the prepared dust sample was digested with a concentrated HNO_3-$HClO_4$-HF-HCl mixture at the ALS Laboratory, Guangzhou. The concentrations of metal(loid)s (i.e., As, Cd, Cr, Cu, Mo, Ni, Pb, Sb and Zn) in the digested solution were determined by an inductively coupled plasma–mass spectrometer (ICP-MS). Duplicate analysis of samples returned an average relative standard deviation (RSD) <6% for all elements. Recovery rates were measured using the Certified Reference Materials (CRM)

GBM908-10 and MRGeo08 with recovery rates ranging 92-104% and 90-107% for all elements, respectively. Correlation between the concentrations of heavy metal(loid)s and magnetic properties were analyzed using the statistical software SPSS 23.0.

2. Results

3.1 Magnetic properties of bulk samples

The magnetic properties of household dust are presented in Table 1. χ of household dust ranges from 50.0×10^{-8} m^3kg^{-1} to 684.2×10^{-8} m^3kg^{-1}, with a mean value of $(187\pm111)\times10^{-8}$ m^3kg^{-1}. χ is significantly correlated with SIRM (Fig. 2a) indicating that χ is dominated by ferri(o)magnetic minerals. Likewise, the mean S_{-300} value of the household dust sample is 96.8 $\pm$2.1 %, which also suggests the dominance of ferri(o)magnetic particles as magnetic carriers. χ_{fd}% ranges from 0.0 to 4.7%, with mean value of 1.7$\pm$1.5%, indicating a small contribution by superparamagnetic (SP, e.g., <30 nm for magnetite) grains to the total magnetic susceptibility (Dearing et al., 1996). χ_{ARM}/SIRM and χ_{ARM}/χ are commonly used as a grain size indicator of magnetic particles. Mean χ_{ARM}/SIRM andχ_{ARM}/χ values of $(17.8\pm5.6)\times10^{-5}$ mA^{-1} and 2.3$\pm$0.8, respectively, suggest that the magnetic grains are predominantly pseudosingle domain (PSD, e.g., 70 nm-10 μm for magnetite) and multidomain (MD, e.g., >10 μm for magnetite) in size (Dekkers, 1997). The bi-plot of SIRM vs χ_{ARM}/SIRM shows that household dust samples with higher SIRM have a coarser grain size, while IMPs of those samples with lower SIRM are finer (Fig. 2b). In addition, a significant positive relationship has been found between χ_{ARM}/SIRM and χ_{ARM}/χ for the household dust, confirming that χ is not significantly influenced by superparamagnetic particles (Fig. 2c). In general, HIRM shows a positive relationship with SIRM, which can enable two groups of samples identified (Fig. 2d).

INSERT TABLE 1 AND FIGURE 2

3.2 Thermomagnetic analysis

The heating curves show a rapid drop in magnetization at around ~585 ℃ indicating that magnetite is the dominant magnetic carrier in our household dust samples (Fig. 3 b, d, f, h).

There is a decline in magnetization between ~300 and 400℃, which probably indicates the conversion of maghemite to hematite (Fig. 3; Deng et al., 2001; Gao et al., 2019). The hump around 500℃ suggests the transformation of weakly paramagnetic minerals to a ferrimagnetic mineral (Fig. 3). Some of the samples show a continuing decline in magnetization beyond ~700℃ on the heating curves. This indicates a second Curie temperature above 700℃ and the presence of metallic iron in the dust (Fig.3 a-b,e-f,g-h; Zhang et al., 2011; Górka-Kostrubiec et al, 2019).

INSERT FIGURE 3

3.3 Day plot and IRM unmixing

The hysteresis loops show closure in the fields beyond 300 mT indicating that the magnetic particles in the household dust in the study primarily consist of low coercivity components such as magnetite (Fig. 4b and d). On the Day plot, the samples are located in the PSD-MD field, which suggests that magnetic grains were coarse (Fig. 4a; Day et al., 1977; Dunlop, 2002).

INSERT FIGURE 4

Unmixing of IRM acquisition curves of the two selected samples D-21 and D-25 according to the Day plot (Fig. 4a) show three components: low-coercivity (~20 mT), medium-coercivity (~50 mT) and high-coercivity (~300 mT) (Figure 4c, e), which usually represent coarse magnetite, fine magnetite/maghemite and hematite, respectively (Kruiver et al., 2001; Yamazaki and Ikehara, 2012). Clearly, the mid-range coercivity component is dominant in terms of the SIRM contribution. As shown in Figure 4, sample D-21, which is located closest to the SD field, has relatively higher coercivities than D-25 does. The latter shifted towards to an MD field and therefore is coarser than sample D-21.

3.4 FORC diagrams

The FORC diagrams for our household dust samples indicate a mixture of low-coercivity magnetite as the main magnetic fraction (Fig. 5). The magnetite consists of a mixture of SD

and PSD (or vortex) sizes (Roberts et al., 2018). The coarsening trend from sample D-21 (Fig. 5a) to D-25 (Fig. 5c) is consistent with the results from the Day plot analysis (Fig. 4).

INSERT FIGURE 5

3.5 SEM and TEM observation

Spherical, irregular sheet-like or blocky magnetic particles with a size ranging 10-50 μm have been found in the household dust samples (Fig. 6). TEM analysis confirms the presence of clumped nano-sized iron-rich particles (10-100 nm) (Fig. 7), which is consistent with the presence of SP and SD grains indicated by the magnetic measurements. Elemental mapping and EDX analysis confirm that the magnetic particles in household dust are mainly composed of Fe and O. Lattice spacing and electron diffraction analysis results are consistent with a magnetite crystals structure (Fig. 7 k, l, o and p). Together these results identify the extremely fine particles (<30 nm) as predominantly magnetite.

INSERT FIGURE 6 AND 7

3.6 Heavy metal(loid)s in bulk samples and their relationships with magnetic properties

The heavy metal(loid)s concentrations and their relationships with magnetic parameters are shown in Table 2 and Table S2. All the analyzed heavy metal(loid)s concentrations (i.e., As, Cd, Cr, Cu, Mo, Ni, Pb, Sb, and Zn) of the household dust samples are higher than those of Shanghai background soil samples (Cheng et al., 2014). The maximum values of heavy metal(loid)s in household dust samples are about 2-76 times the values of background soil. In general, χ_{lf}, χ_{ARM}, SIRM correlate with Mo, Ni and Sb, while HIRM is significantly correlated with As, Mo, Pb and Sb (Table 2).

INSERT TABLE 2

3. Discussion

4.1 Mineral composition and sources based on magnetic measurements

Our analysis indicates that magnetite is the dominant magnetic mineral in the dust collected from 40 Shanghai homes. The thermomagnetic data and IRM unmixing analysis also suggest the presence of hematite and maghemite (Fig. 3 and 4). The decrease in magnetization up to 700 ℃ observed in sample D-2 suggests the presence of metallic Fe (Fig. 3 a-b, e-f,g-h; Fig. 6 g-l; Fig. S1 d-f).

Compared to total suspended particles (TSP), street dust and urban topsoil in Shanghai (e.g., Shu et al., 2000, 2001; Hu et al., 2007; Zhang et al., 2011; Wang et al., 2018, 2019), the concentrations of ferri(o)magnetic minerals (e.g., magnetite) in household dust are higher than those of urban topsoil, but lower than those of street dust, TSP from an industrial zone and dust from subway platforms (Table 1; Fig. 2a). In comparison to the Shanghai background soil, household dust samples have a higher concentration of not only ferri(o)magnetic minerals but antiferromagnetic minerals (e.g., hematite) (Fig. 2d). The relationship between HIRM and SIRM shown in Fig. 2d suggests that high-coercivity magnetic mineral (e.g., hematite) of household dust is a mixture of Shanghai background soil with traffic and industrial emissions. Street dust, TSP samples from an industrial zone and dust from subway platforms are enriched with coarser ferri(o)magnetic particles, while the grain size of the IMPs in household dust is finer (Fig. 2b). This implies that the coarser particles of street dust and airborne particulates emitted by industrial activities (e.g., coal combustion and metallurgical manufacturing) are selectively removed during transport from their sources into the indoor environment (Fig.2 b, c). Meanwhile, most of household dust samples have coarser IMPs than the urban topsoil (Fig. 2b, c), suggesting that track-in activity is a possible transport pathway of soil particles into the indoor environment in addition to the resuspension. In summary, magnetic properties suggest that indoor dust has a mixture source of natural and anthropogenic origin (Fig. 2). Street dust and airborne particulates emitted by industrial activities and traffic seems to make a considerable contribution to household dust in the city according to the Fig. 2.

4.2 Identification of sources in consideration of SEM/TEM images and geochemical data

The SEM images (Fig. 6 g-l; Fig. S1 d-f) further confirm metallic Fe particles in the household dust, which is consistent with the thermomagnetic results. These metallic Fe particles are irregular sheetlike or blocky and reported by other studies (Zhang, 2011; Moreno et al., 2015; Górka-Kostrubiec et al., 2015; Jeleńska et al., 2017; Górka-Kostrubiec and Szczepaniak, 2017). Jeleńska et al., (2017) found angular, metallic Fe particles in office dust in Warsaw (Poland) and considered that these particles were possibly generated by the abrasion of vehicle suspension components. The EDX analysis shows that metallic Fe particles also contain other heavy metals, such as Cr, Cu and Mn (Fig. 6c; Fig. S1 d-f). Previous studies indicate that elements Cr and Cu could be used as key tracers of non-exhaust vehicle emission (e.g., abrasion of brake wear) (Adamiec et al., 2016; Ozaki et al., 2004). Scratches, likely caused by the braking are clearly observed on the surface of the metallic iron particles (Fig.6 g-i). Therefore, the irregular sheet like or blocky metallic Fe particles are likely sourced from abrasion of brake wear.

In addition to the irregular sheet like and blocky metallic Fe particles, spherical IMPs are also shown in the SEM images (Fig. 6; Fig. S1). These particles have a wide particle size range (2-30 μm) (Fig. 6; Fig. S1), which is also consistent with the size of PSD/MD magnetic grains. These spherical IMPs in the indoor dust are similar to magnetic particles in fly ash that are generated during coal combustion (e.g., Wang et al., 2019; Zhang et al., 2020). Previous studies have revealed that spherical, IMPs occur in subway dust, topsoil and street dust in Shanghai, implying a widespread distribution of fly ash in the urban environment (Zhang, 2011; Yang et al., 2016; Wang et al., 2019). This suggests that coal combustion, in addition to non-exhaust vehicle emission (e.g., abrasion of brake wear), contributes to the IMPs load of the dust in homes in Shanghai.

Considering the geochemical data, the enrichment of Sb in household dust samples (Table 2) supports the view that non-exhaust vehicle emissions (e.g. brake wear, tire wear) contributes to household dust according to Yan et al., (2020). The enrichment of Mo (Table 2), which is regarded as an indicator of coal combustion (Zhu et al., 2013), also suggests that the coal combustion contributes to the household dust samples. The association between HIRM and As, Mo, Pb and Sb implies that the high-coercivity magnetic particles (e.g., hematite) are

contributed by industrial emission (e.g., coal combustion, metallurgical manufacturing) and non-exhaust vehicle emissions according to previous studies (Zhu et al., 2013; Yan et al., 2020; Teran et al., 2020). Moreover, the Pb isotopic data of household dust samples presented in another manuscript under preparation shows similar compositions with outdoor PM_{10}/$PM_{2.5}$ and urban surface soil (Fig. S2), which confirms the contribution of outdoor air, street dust and urban topsoil to household dust. Tobacco smoking and domestic biomass fuels consumption (e.g., coal, wood) are usually considered as indoor sources of IMPs (e.g., Jordanova et al., 2006; Maher et al., 2021), but are not likely to make a considerable contributions to household dust IMPs in this study. The investigated homes in this study are non-smoking. Meanwhile, in these homes cooking is undertaken using natural gas and therefore domestic sources of IMPs are minor in this study.

Above all, a multiple lines of evidence approach using a combination of magnetic methods, SEM/TEM and geochemical data reveals a mixed magnetic mineralogy in our samples, which is consistent with the nature of Shanghai's characteristics as a city with heavy traffic and significant emissions from industrial (e.g., coal combustion and metallurgical manufacturing) emissions. The difference in IMPs in particle size and mineral assemblage may be due to local environmental conditions such as the surroundings of particular houses e.g., the proximity to main roads, screening by other structures, age and ventilation of individual houses.

4.3 Comparison with indoor dust elsewhere

In comparison to indoor dust characteristics determined in other cities (Jordanova et al., 2012; Górka-Kostrubiec et al., 2014; Górka-Kostrubiec, 2015; Kelepertzis et al., 2019, 2021; Maher et al., 2021), Shanghai has similar χ values to those reported in Athens (Greece) (Kelepertzis et al., 2019) and Warsaw (Poland) (Górka-Kostrubiec, 2015), but lower levels than in Volos (Greece), Sofia and Burgas (Bulgaria) (Jordanova et al., 2012; Kelepertzis et al., 2021). However, dust in Warsaw has a higher proportion of iron, as indicated by the stronger decline in χ between 580°C and 780°C in the thermomagnetic curves (Górka-Kostrubiec, 2015).

Using Ms as an indicator of magnetic mineral concentration, this study found that indoor dust of Shanghai has higher values than indoor $PM_{2.5}$ and $PM_{10\text{-}2.5}$ in Ireland (Maher et al., 2021).

Furthermore, according to the differences in mean χ_{ARM}/SIRM and χ_{ARM}/χ and the SEM observations of spherical particles (Fig. 6; Fig. S1), the grain size of magnetic mineral in dust in Shanghai is finer than that of indoor dust in Warsaw (Table 3). A possible explanation for this difference may be the distance between the sampling sites and the emission sources. In Shanghai, the dust was mainly collected in Putuo District, where there are no significant local industrial contamination sources. In Warsaw, indoor dust was collected from the city center close to a power plant or suburbs 10 km from the city center (Górka-Kostrubiec, 2015).

INSERT TABLE 3

4.4 Implication of environmental health

The association between magnetic properties and heavy metal(loid)s (Table S2) suggests that heavy metal(loid)s were emitted into the environment along with the IMPs or absorbed by these particles (Zhang et al., 2018), which may cause negative effects on human health. Moreover, some studies have shown that fine and ultrafine magnetic particles in dust can also be damaging to human health through neurodegeneration and cardiovascular disease (Singh et al., 2010; Maher et al., 2016, 2021; Miller et al., 2017; Sutto, 2018; Calderón-Garcidueñas et al., 2019). The potential toxicity of magnetic particles is directly related to concentration, particle size and mineral species. Using Ms as an indicator of concentration of magnetite, and assuming that magnetite accounts for 100% of the magnetic particles, it is estimated that household magnetite concentration in Shanghai is approximately 0.3 wt%. Although this value could be overestimated, because of the presence of iron in our samples, this rough estimation is in the same range as the magnetite concentration reported for $PM_{2.5}$ in Beijing (Zhang et al., 2020). Magnetic minerals of different sizes and compositions may present different toxicity risks. Particle size determines whether magnetic particles can cross the blood-brain barrier, the placenta barrier, or enter cells through pinocytosis. We found fine-grained magnetic particles of <~100 nm in our dust samples. Dearing et al. (1997) suggests that χ_{fd}% may be used semi-quantitatively to estimate the proportion of SP in samples, where values of 2, 8 and 10 % are roughly equivalent to >10, >50 and >75 % of frequency-dependent SP grains, respectively. It is estimated that SP grains accounted for

0~20% of total magnetic particles in this study (Fig. S3). The general positive relationship between the proportion of SP grains, reflected by χ_f/Ms and χ (Fig. 8; Hunt al., 1995), implies that more ultra-fine nanoparticles are present in the more magnetic samples. Magnetic measurements can provide an efficient semi-quantitative characterization of iron-containing particles in a rapid and cost-effective way. The significant relationships between concentration-related magnetic parameters and metal(loid)s in the household dust (Table S2) confirms that a magnetic method can be used for monitoring and assessing metal pollution status in urban environment. Furthermore, this approach, in combination with other chemical methods, has great potential in the assessment of the toxicity of indoor dust, including its nano-particle size range.

4. Conclusion

Magnetic measurement and SEM/TEM observations were used to characterize the magnetic mineralogy of dust from homes in Shanghai. The results show that the magnetic particles in this dust are dominated by magnetite, together with varying levels of maghemite, hematite and metallic Fe. The estimated magnetite content of our dust samples is 0.3%. Most of the IMPs in our samples are larger than 100 nm. However, nano-sized IMPs with a size of <~100 nm are evident and tend to increase proportionately in samples with a higher magnetic particle abundance. A multiple lines of evidence approach using a combination of magnetic measurements, geochemical analyses and SEM/TEM observation revealed that industrial emission (i.e., coal combustion and metallurgical manufacturing) and non-exhaust traffic activity, make a considerable contribution to household dust in Shanghai. Such an approach can help to establish more precisely the sources of household dust particles and could be applied to other indoor contexts and further urban environments.

Acknowledgments

This work was supported by the grants from the Basic Research Foundation of the National Commonwealth Research Institute (No. PM-zx703–202104-055), China Postdoctoral Science Foundation (2019M661539), Shanghai Post-doctoral Excellence Program (2018034) and the National Natural Science Foundation of China (41976158). Dr. Guan Wang is thanked for providing the HIRM values of Shanghai urban topsoil. We thank Editor Dr. Meiping Tong

and the anonymous reviewers whose constructive comments/suggestions improved this manuscript. We also thank Chenyao Yan for her help with experimental analysis.

References

Adamiec, E., Jarosz-Krzeminska, E., Wieszała, R., 2016. Heavy metals from non-exhaust vehicle emissions in urban and motorway road dusts. Environ. Monit. Assess. 188, 369. https://doi.org/10.1007/s10661-016-5377-1.

Ao, J. J., Yuan, T., Ma, Y. N., Gao, L., Ni, N., Li, D., 2017. Identification, characteristics and human exposure assessments of triclosan, bisphenol- A, and four commonly used organic UV filters in indoor dust collected from Shanghai, China. Chemosphere 184, 575-583. https://doi.org/10.1016/j.chemosphere.2017.06.033.

Bloemendal, J., King, J. W., Hall, F. R., Dou, S. J., 1992. Rock magnetism of Late Neogene and Pleistocene deep-sea sediments: Relationship to sediment source, diagenetic processes, and sediment lithology. J. Geophys. Res. 97, 4361-4375.

Bloemendal, J., Lamb, B., King, L., 1988. Paleoenvironmental implications of rock-magnetic properties of Lake Quaternary sediment cores from the eastern equatorial Atlantic. Paleoceanography, 3, 61-87.

Bu, Z. M., Xu, X. X., Xu, Q., Mmereki, D., Wang, J. H., Cheng, Z., Li, K., Dong, C., 2020. Indoor polybrominated diphenyl ethers in urban China: An exposure and risk assessment based on settled dust from selected urban regions. Sci. Total Environ. 714, 136808. https://doi.org/10.1016/j.scitotenv.2020.136808.

Calderón-Garcidueñas, L., González-Maciel, A., Mukherjee, P. S., Reynoso-Robles, R., Pérez-Guillé, B., Gayosso-Chávez, C., Torres-Jardón, R., Cross, J. V., Ahmed, I. A. M., Karloukovski, V. V., Maher, B. A., 2019. Combustion- and friction-derived magnetic air pollution nanoparticles in human hearts. Environ. Res. 176, 108567. https://doi.org/10.1016/j.envres.2019.108567.

Chaparro, M. A., Suresh, G., Chaparro, M. A., Ramasamy, V., Sundarrajan, M., 2017. Magnetic assessment and pollution status of beach sediments from Kerala coast (southwestern India). Mar. Pollut. Bull. 117, 171-177. https://doi.org/10.1016/j.marpolbul.2017.01.044.

Cui, G. P., Zhou, L. P., Dearing, J., 2016. Granulometric and magnetic properties of deposited particles in the Beijing subway and the implications for air quality management. Sci. Total Environ. 568, 1059-1068. https://doi.org/10.1016/j.scitotenv.2016.06.154.

Cheng, H. X., Li, K., Li, M., Yang, K., Liu, F. Cheng, X. M., 2014. Geochemical background and baseline value of chemical elements in urban soil in China. Ear. Sci. Fro. 21, 265-306 (in Chinese with English abstract). https://doi.org/10.13745/j.esf.2014.03.028.

Day, R., Fuller, M., Schmidt, V. A., 1977. Hysteresis properties of titanomagnetites-grain-size and compositional dependence. Phys. Earth Planet. Int. 13, 260-267.

Dearing, J. A., Bird, P. M., Dann, R. J. L., Benjamin, S. F., 1997. Secondary ferrimagnetic minerals in Welsh soils: a comparison of mineral magnetic detection methods and implications for minerals formation. Geophys. J. Int. 130, 727-736. https://doi.org/10.1111/j.1365-246X.1997.tb01867.x.

Dearing, J. A., Hay, K. L., Baban, S. M. J., Huddleston, A. S., Wellington, E. M. H., Loveland, P. J., 1996. Magnetic susceptibility of soil: an evaluation of conflicting theories using a national data set. J. Geophys. Int. 127, 728-734. https://doi.org/10.1111/j.1365-246X.1996.tb04051.x.

Deng, C., Zhu, R., Jackson, M., Verosub, K., Singer, M., 2001. Variability of the temperature-dependent susceptibility of the Holocene eolian deposits in the Chinese Loess Plateau: A pedogenesis indicator. Phys. Chem. Earth. 26, 873-878. https://doi.org/10.1016/S1464-1895(01)00135-1.

Dunlop, D, J. 2002. Theory and application of the Day plot (Mrs/Ms versus Hcr/Hc) 1. Theoretical curves and tests using titanomagnetite data. J. Geophys. Res. 107, 2056. https://doi.org/10.1029/2001JB000486.

Dekkers, M. J. 1997. Environmental magnetism: An introduction, Geol. Mijnbouw. 76, 163-182. https://doi.org/10.1023/A:1003122305503.

Egli, R., 2013. VARIFORC: An optimized protocol for calculating non-regular first-order reversal curve (FORC) diagrams. Glob. Planet. Change. 110, 302-320. https://doi.org/10.1016/j.gloplacha.2013.08.003.

Ge, C., Zhang, W., Dong, C., Wang, F., Feng, H., Qu, J., Yu, L., 2017. Tracing sediment erosion in the Yangtze River subaqueous delta using magnetic methods. J. Geophys Res. Earth Surf. 122, 2064-2078. https://doi.org/10.1002/2017JF004403.

Gao, X. B., Hao, Q. Z., Oldfield, F., Bloemendal, J., Deng, C. L., Wang, L., Song, Y., Ge, J. Y., Wu, H. B, Xun, B., Li, F. J, Han, L., Fu, Y., Guo, Z. T., 2019. New high-temperature dependence of magnetic susceptibility-based climofunction for quantifying paleoprecipitation from Chinese loess. Geochem. Geophys. Geosyst. 20, 4273-4291. https://doi.org/10.1029/2019GC008401.

Gonet, T., Maher, B. A., 2019. Airborne, Vehicle-derived Fe-bearing nanoparticles in the urban environment: A Review. Environ. Sci. Technol. 53, 9970-9991. https://doi.org/10.1021/acs.est.9b01505.

Górka-Kostrubiec, B., 2015. The magnetic properties of indoor dust fractions as markers of air pollution inside buildings. Build. Environ. 90, 186-195. https://doi.org/10.1016/j.buildenv.2015.03.034.

Górka-Kostrubiec, B., Jeleńska, M., Król, E., 2014. Magnetic signature of indoor air pollution: household dust study. Acta Geophys. 62, 1478-1503. https://doi.org/10.2478/s11600-014-0238-1.

Górka-Kostrubiec, B., Szczepaniak-Wnuk, I., 2017. Magnetic study of a mixture of magnetite and metallic iron in door dust samples. Air Qual. Atmos. Health. 10, 105-116. https://doi.org/10.1007/s11869-016-0412-5.

Górka-Kostrubiec, B., Werner, T., Dytlow, S., Szczepaniak-Wnuk, I., Jeleńska, M., Hanc-Kuczkowska,. A., 2019. Detection of metallic iron in urban dust by using high-temperature measurements supplemented with microscopic observations and Mössbauer spectra. J. Appl. Geophys. 166, 89-102. https://doi.org/10.1016/j.jappgeo.2019.04.022.

Harrison, R. J., Feinberg, J. M., 2008. FORCinel: An improved algorithm for calculating first-order reversal curve distributions using locally weighted regression smoothing. Geochem. Geophys. Geosyst. 9, Q5016. https://doi.org/10.1029/2008GC001987.

Hofman, J., Maher, B. A., Muxworthy, A. R., Wuyts, K., Castanheiro, A., Samson, R., 2017. Biomagnetic Monitoring of Atmospheric Pollution: A Review of Magnetic Signatures from Biological Sensors. Environ. Sci. Technol. 51, 6648-6664. https://doi.org/10.1021/acs.est.7b00832.

Hatfield, R. G., Wheeler, B. H., Reilly, B. T., Stoner, J. S., Housen, B. A., 2019. Particle size specific magnetic properties across the Norwegian-Greenland Seas: insights into the influence of sediment source and texture on bulk magnetic records. Geochem. Geophys. Geosyst. 20, 1004-1025. https://doi.org/10.1029/2018GC007894.

Hu, X. F., Su, Y., Ye, R., Li, X. Q., Zhang, G. L., 2007. Magnetic properties of the urban soils in Shanghai and their environmental implications. Catena. 70, 428-436. https://doi.org/10.1016/j.catena.2006.11.010.

Hunt, C. P., Banerjee, S. K., Han, J., Solheid, P. A., Oches, E., Sun, W. W., Liu, T. S., 1995. Rock-magnetic proxies of climate change in the loess-palaeosol sequences of the western Loess Plateau of China. Geophys. J. Int. 123, 232-244. https://doi.org/10.1111/j.1365-246X.1995.tb06672.x.

Jaffar, S. T. A., Chen, L., Younas, H., Ahmad, N., 2017. Heavy metals pollution assessment in correlation with magnetic susceptibility in topsoils of Shanghai. Environ. Earth Sci. 76, 277. https://doi.org/10.1007/s12665-017-6598-5.

Jeleńska, M., Górka-Kostrubiec B, Werner, T., Kádziałko-Hofmokl, M., Szczepaniak-Wnuk, I., Gonet, T., Szwarczewski, P., 2017. Evaluation of indoor/outdoor urban air pollution by magnetic, chemical and microscopic studies. Atmos. Pollut. Res. 8, 754-766. https://doi.org/10.1016/j.apr.2017.01.006.

Jordanova, D., Jordanova, N., Lanos, P., Petrov, P., Tsacheva. T., 2012. Magnetism of outdoor and indoor settled dust and its utilization as a tool for revealing the effect of elevated particulate air pollution on cardiovascular mortality. Geochem. Geophys. Geosyst. 13, 1525-2027. https://doi.org/10.1029/2012GC004160.

Jordanova, N., Jordanova, D., Henry, B., Goff, M L., Dimov, D., Tsacheva, T., 2006. Magnetism of cigarette ashes. J. Magn. Magn. Mater. 301, 50-66.

Jung, H. J., Kim, B., Malek, M. A., Koo, Y. S., Jung, J. H., Son, Y. S., Kim, J. C., Kim, H., Ro, C., 2012. Chemical speciation of size-segregated floor dusts and airborne magnetic particles collected at underground subway stations in Seoul, Korea. J. Hazard. Mater. 213-214, 331-340. https://doi.org/10.1016/j.jhazmat.2012.02.006.

Kelepertzis, E., Argyraki, A., Botsou, F., Aidona, E., Szabó, Á., Szabó, C., 2019. Tracking the occurrence of anthropogenic magnetic particles and potentially toxic elements (PTEs) in house dust using magnetic and geochemical analyses. Environ. Pollut. 245, 909-920. https://doi.org/10.1016/j.envpol.2018.11.072.

Kelepertzis, E., Chrastný, V., Botsou, F., Sigala, E., Kypritidou, Z., Komárek, M., Skordas, K., Argyraki, A., 2021. Tracing the sources of bioaccessible metal(loid)s in urban environments: A multidisciplinary approach. Sci. Total Environ. 771, 144827. https://doi.org/10.1016/j.scitotenv.2020.144827.

Kruiver, P. P., Dekkers, M. J., Heslop, D., 2001. Quantification of magnetic coercivity components by the analysis of acquisition curves of isothermal remanent magnetization. Earth Planet. Sci. Lett. 189, 269-276. https://doi.org/10.1016/S0012-821X(01)00367-3.

Li, L., Qiu, Y. L., Gustafesson, Å., Krais, A. M., Weiss, J. M., Lundh, T., Bergman, Å., 2019. Characterization of residential household dust from Shanghai by particle size and analysis of organophosphorus flame retardants and metals. Environ. Sci. Eur. 31, 94. https://doi.org/10.1186/s12302-019-0279-9.

Li, M. K., Zhu, S. Y., Ouyang, T. P., Tang, J. H., Tang, Z. H., 2021. Magnetic properties of the surface sediments in the Yellow River Estuary and Laizhou Bay, Bohai Sea, China: Implications for monitoring heavy metals. J. Hazard. Mater. 410, 124579. https://doi.org/10.1016/j.jhazmat.2020.124579.

Liu, N. M., Miyashita, L., Maher, B. A., McPhail, G., Jones, C. J. P., Barratt, B., Thangaratinam, S., Karloukovski, V., Ahmed, I. A., Aslam, Z., Grigg, J., 2021. Evidence for the presence of air pollution nanoparticles in placental tissue cells. Sci. Total Environ. 751, 142235. https://doi.org/10.1016/j.scitotenv.2020.142235.

Lu, D., Luo, Q., Chen, R., Zhuansun, Y., Jiang, J., Wang, W., Yang, X., Zhang, L., Liu, X., Li, F., Liu, Q., Jiang, G., 2020. Chemical multi- fingerprinting of exogenous ultrafine particles in human serum and pleural effusion. Nat. Commun. 11, 2567. https://doi.org/10.1038/s41467-020-16427-x.

Maher, B. A., 1986. Characterisation of soils by mineral magnetic measurements. Phys. Earth Planet. Int. 42, 76-92.

Maher, B. A., Ahmed, I. A. M., Karloukovski, V., MacLaren, D. A., Foulds, P. G., Allsop, D., Mann, D. M. A., Torres-Jardón, R., Calderon-Garciduena, L., 2016. Magnetite pollution

nanoparticles in the human brain. PNAS. 113, 10797-10801. https://doi.org/10.1073/pnas.1605941113.

Maher, B. A., O'Sullivan, V., Feeney, J., Gonet, T., Kenny, R. A., 2021. Indoor particulate air pollution from open fires and the cognitive function of older people. Environ. Res. 192, 110298. https://doi.org/10.1016/j.envres.2020.110298.

Maher, B. A., Thompson, R. (Eds.), 1999, Quaternary Climates, Environments and Magnetism, 390 pp., Cambridge Univ. Press, Cambridge, U. K., doi:10.1017/ CBO9780511535635.

Mitchell, R., Maher, B. A., 2009. Evaluation and application of biomagnetic monitoring of traffic-derived particulate pollution. Atmos. Environ. 43, 2095-2103. https://doi.org/10.1016/j.atmosenv.2009.01.042.

Moreno, T., Martins,V., Querol, X., Jones, T., BéruBé, K., Minguillón, M. C., Amato, F., Capdevila, M., Miguel, de E., Centelles, S., Gibbons, W., 2015. A new look at inhalable metalliferous airborne particles on rail subway platforms. Sci. Total Environ. 505, 367-375. https://doi.org/10.1016/j.scitotenv.2014.10.013.

Ozaki, H., Watanabe, I., Kuno, K., 2004. Investigation of the heavy metal sources in relation to automobiles. Water, Air, Soil Pollut. 157, 209-223. https://doi.org/10.1023/B:WATE.0000038897.63818.f7.

Pattammattel, A., Leppert, V. J. Aronstein, P., Robinson, M., Mousavi, A., Sioutas, C., Forman, H. J. O'Day., P. A., 2021. Iron speciation in particulate matter ($PM_{2.5}$) from urban Los Angeles using spectro-microscopy methods. Atmos. Environ. 245, 117988. https://doi.org/10.1016/j.atmosenv.2020.117988.

Peng, H., Yang, Y., Liu, M., Zhou, J. L., 2012. PAHs in indoor dust samples in Shanghai's universities: levels, sources and human exposure. Environ. Geochem. Health. 34, 587-596. https://doi.org/10.1007/s10653-012-9456-0.

Petersen, N., von Dobeneck, T., Vali, H., 1986. Fossil bacterial magnetite in deep-sea sediments from the South Atlantic Ocean. Nature 320, 611–614.

Petrovsky, E., Ellwood, B. B., 1999. Magnetic monitoring of air, land and water pollution. In: Maher, B. A. and Thompson, R. (eds) Quaternary Climates, Environments, and Magnetism. Cambridge University Press, Cambridge, 278–322.

Roberts, A. P., Zhao, X., Harrison, R. J., Heslop, D., Muxworthy, A. R., Rowan, C. J., Larrasonaña, J. C., Florindo, F., 2018. Signatures of reductive magnetic mineral diagenesis from unmixing of first-order reversal curves. J. Geophys. Res: Solid Earth. 123, 4500-4522. https://doi.org/10.1029/2018JB015706.

Shanghai Municipal Bureau of Statistics, NBS Survey Office in Shanghai, 2019. Shanghai Statistical Yearbook (2019). Beijing: China Statistics Press.

Shu, J., Dearing, J. A., Morse, A. P., Yu, L. Z., Li, C., 2000. Magnetic Properties of Daily Sampled Total Suspended Particulates in Shanghai. Environ. Sci. Technol. 34, 2393-2400. https://doi.org/10.1021/es9910964.

Shu, J., Dearing, J. A., Morse, A. P., Yu, L. Z., Yuan, N., 2001. Determining the sources of atmospheric particles in Shanghai, China, from magnetic and geochemical properties. Atmos. Environ. 35, 2615-2625. https://doi.org/10.1016/S1352-2310(00)00454-4.

Singh, N., Jenkins, G. J. S., Asadi, R., Doak, S. H., 2010. Potential toxicity of superparamagnetic iron oxide naoparticles (SPION). Nano Rev. 1, 5358. https://doi.org/10.3402/nano.v1i0.5358.

Snowball, I., Hounslow, M. W., Nilsson, A., 2014. Geomagnetic and mineral magnetic characterization of the Anthropocene. In: Waters, C. N., Zalasiewicz, J. A., Williams, M., Ellis,M. A. & Snelling, A. M. (eds). A stratigraphical basis for the Anthropocene. Geological Society, London, Special Publications, 395, 119-141. https://doi.org/10.1144/sp395.13.

Sutto, T., E., 2018. Magnetite fine particle and nanoparticle environmental contamination from industrial uses of coal. Environ. Pollut. 243, 528-533. https://doi.org/10.1016/j.envpol.2018.08.080.

Turner, A., 2011. Oral bioaccessibility of trace metals in household dust: a review. Environ. Geochem. Health. 33, 331-341. https://doi.org/10.1007/s10653-011-9386-2.

Teran, K., Žibret, G., Fanetti, M. 2020. Impact of urbanization and steel mill emissions on elemental composition of street dust and corresponding particle characterization. J. Hazard. Mater. 384, 120963. https://doi.org/10.1016/j.jhazmat.2019.120963.

Wang, F., Zhang, W. G., Nian, X. M., Roberts, A. P., Zhao, X., Shang, Y., Ge, C., Dong, Y., 2020. Magnetic evidence for Yellow River sediment in the late Holocene deposit of the Yangtze River Delta, China. Mar. Geol. 427, 106274. https://doi.org/10.1016/j.margeo.2020.106274.

Wang, G., Chen, J., Zhang, W. G., Ren, F. F., Chen, Y. Y, Fang, A. D., Ma, L. J., 2019. Magnetic properties of street dust in Shanghai, China and its relationship to anthropogenic activities. Environ. Pollut. 255, 113214. https://doi.org/10.1016/j.envpol.2019.113214.

Wang, G., Chen, Y. Y., Xia, D. S., Ren, F. F., Fang, A. D., Ma, L. J., 2018. Magnetic property of urban topsoil and its implication of heavy metal pollution in Shanghai. Acta Scientiae Cirumstantiae. 38, 3302-3312. (in Chinese with English abstract). https://doi.org/10.13671/j.hjkxxb.2018.0086.

Wang, S., Liu, J., Li, J., Xu, G., Qiu, J., Chen, B., 2020. Environmental magnetic parameter characteristics as indicators of heavy metal pollution in the surface sediments off the Zhoushan Islands in the East China Sea. Mar. Pollut. Bull. 150, 110462. https://doi.org/10.1016/j.marpolbul.2019.110642.

Yamazaki, T., Ikehara, M., 2012. Origin of magnetic mineral concentration variation in the Southern Ocean. Paleoceanography. 27, PA2206. https://doi.org/10.1029/2011PA002271.

Yang, Y., Vance, M., Tou, F.Y., Tiwari, A., Liu, M., Hochella Jr, M. F., 2016. Nanoparticles in road dust from impervious urban surfaces: distribution, identification, and environmental implications. Environ.-Sci. Nano. 3, 534-544. https://doi.org/10.1039/C6EN00056H.

Yan, G., Mao, L. C., Liu, S. X., Mao, Y., Ye, H., Huang, T. S., Li, F. P., Chen, L., 2018. Enrichment and sources of trace metals in roadside soils in Shanghai, China: A case study of two urban/rural roads. Sci. Total Environ. 631-632, 942-950. https://doi.org/10.1016/j.scitotenv.2018.02.340.

Yan, G., Mao, L. C., Jiang, B. Y., Chen, X. R. Gao, Y. Chen, C. Z., Li, F. P., Chen, L., 2020. The source, apportionment, pollution characteristic and mobility of Sb in roadside soil affected by traffic and industrial activities. J. Hazard. Mater. 384, 121352. https://doi.org/10.1016/j.jhazmat.2019.121352.

Zhang, Q. H., Lu, D. W., Wang, D. Y., Yang, X. Z., Zuo, P. J., Yang, H., Fu, Q., Liu, Q., Jiang, G. B., 2020. Separation and tracing of anthropogenic magnetite nanoparticles in the urban at atmosphere. Environ. Sci. Technol. 54, 9274-9284. https://doi.org/10.1021/acs.est.0c01841.

Zhang, W. G., Jiang, H., Dong, C., Yan, Q., Yu, L., Yu, Y., 2011. Magnetic and geochemical characterization of iron pollution in subway dusts in Shanghai, China. Geochem. Geophy. Geosy. 12, Q06Z25. http://dx.doi.org/10.1029/2011GC003524.

Zhao, L. M., Zhang, Y. Y., Deng, Y. Y., Jian, K., Li, J. H., Ya, M. L., Su, G. Y., 2020. Traditional and emerging organophosphate esters (OPEs) in indoor dust of Nanjing, eastern China: Occurrence, human exposure, and risk assessment. Sci. Total Environ. 712, 136494. http://dx.doi.org/10.1016/j.scitotenv.2020.136494.

Zhao, X. G., Li, Z. L., Wang, D. L., Tao, Y., Qiao, F. Y., Lei, L. M., Huang, J., Ting, Z, 2021. Characteristics, source apportionment and health risk assessment of heavy metals exposure via household dust from six cities in China. Sci. Total Environ. 762, 143126. https://doi.org/10.1016/j.scitotenv.2020.143126.

Zhu, Z. M., Sun, G. Y., Bi, X. Y., Li, Z. G., Yu, G. H., 2013. Identification of trace metal pollution in urban dust from kindergartens using magnetic, geochemical and lead isotopic analyses. Atmos. Environ. 77, 9-15. http://dx.doi.org/10.1016/j.atmosenv.2013.04.053.

Figure captions

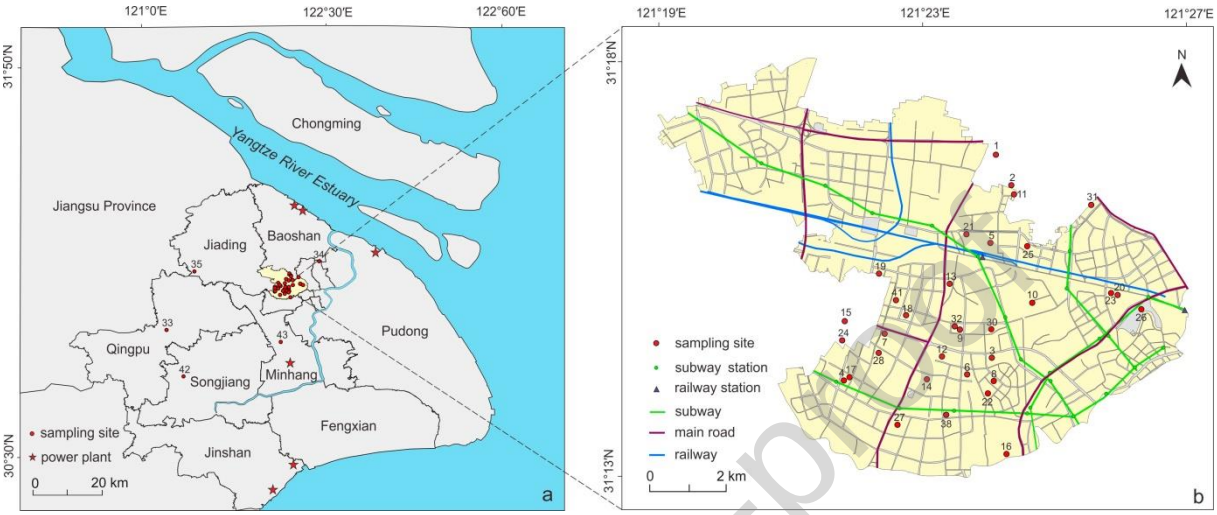

Fig. 1 Map showing the location of sampling sites in Shanghai (a) and Putuo district (b).

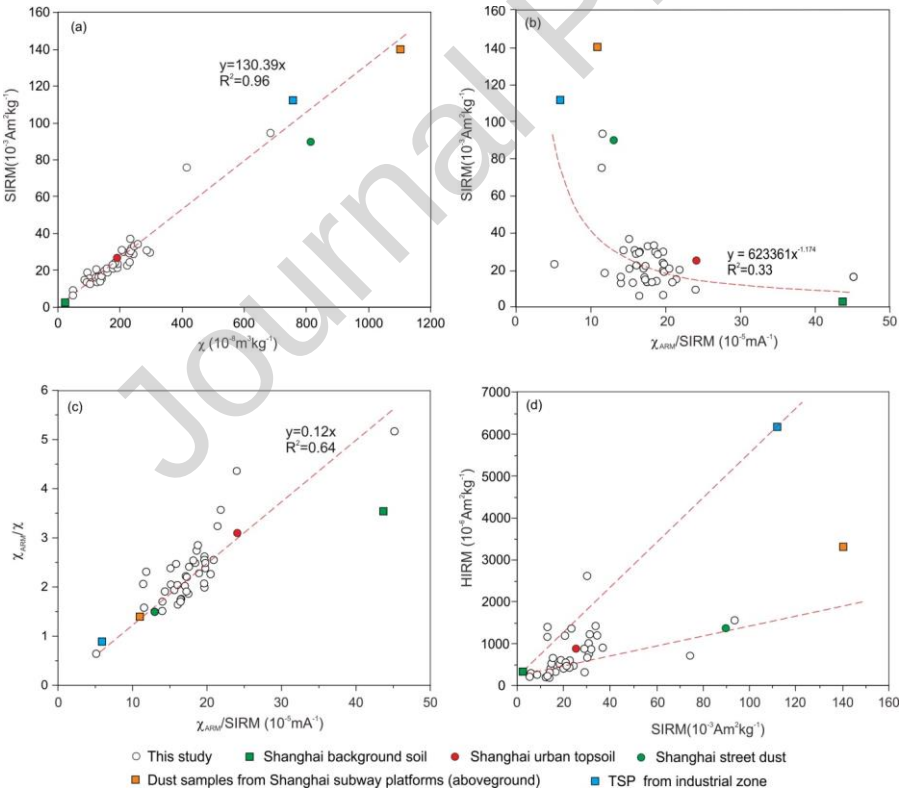

Fig.2 Relationship between magnetic susceptibility (χ) and SIRM (a), SIRM and χ_{ARM}/SIRM (b), χ_{ARM}/χ and χ_{ARM}/SIRM (c), SIRM and HIRM (d) in Shanghai household dust and comparison with outdoor dust and soil in Shanghai, e.g., Shanghai background soil (Hu et al.,

2007); Shanghai urban topsoil (Wang et al., 2018); Shanghai street dust (Wang et al., 2019); Dust samples from Shanghai subway platforms (aboveground) (Zhang et al., 2011); TSP from industrial zone (sites 6-11) (e.g., coal combustion and metallurgical manufacturing) (Shu et al., 2000).

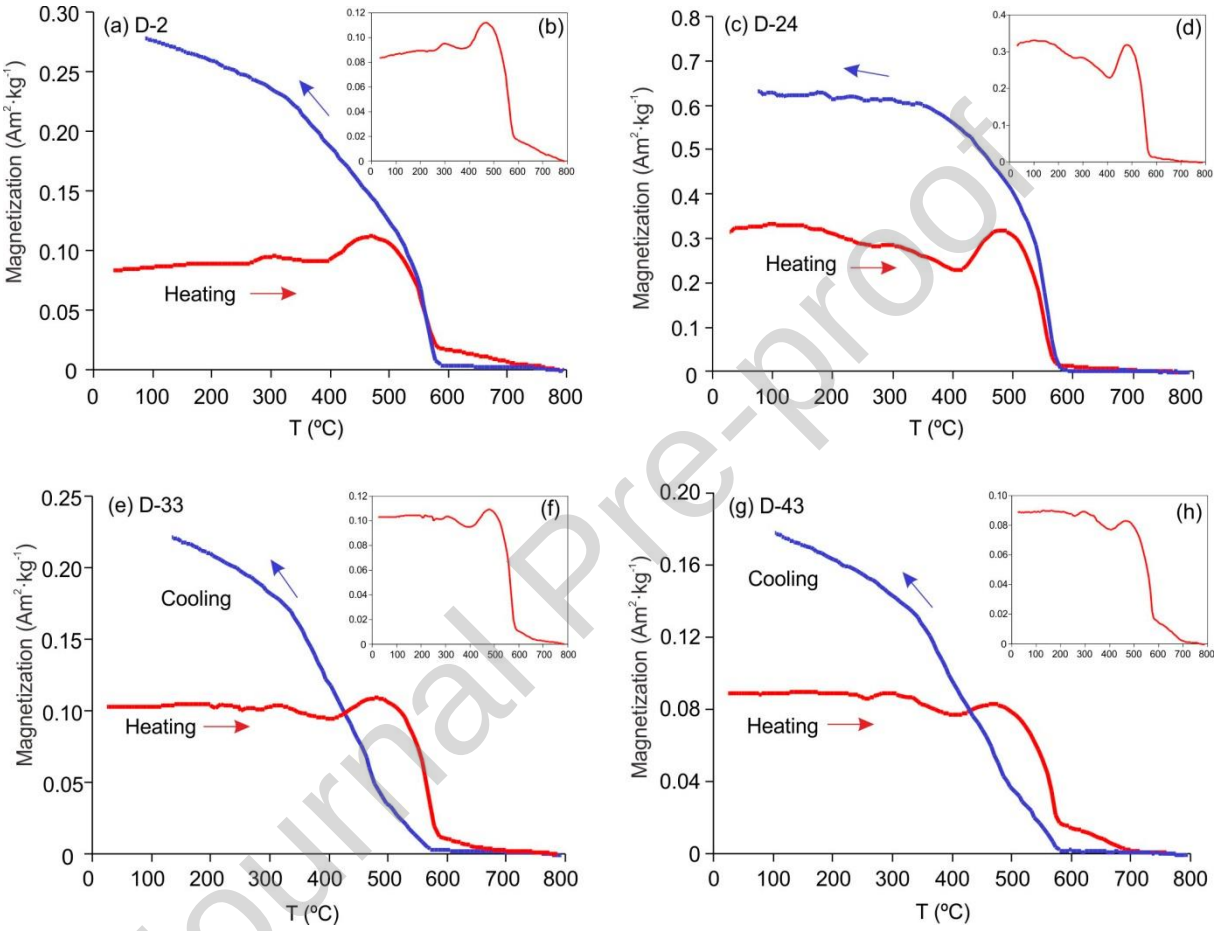

Fig.3 Representative temperature-dependent magnetization (a-h) curves of selected household dust samples from Shanghai with the red and blue lines representing heating and cooling processes, respectively.

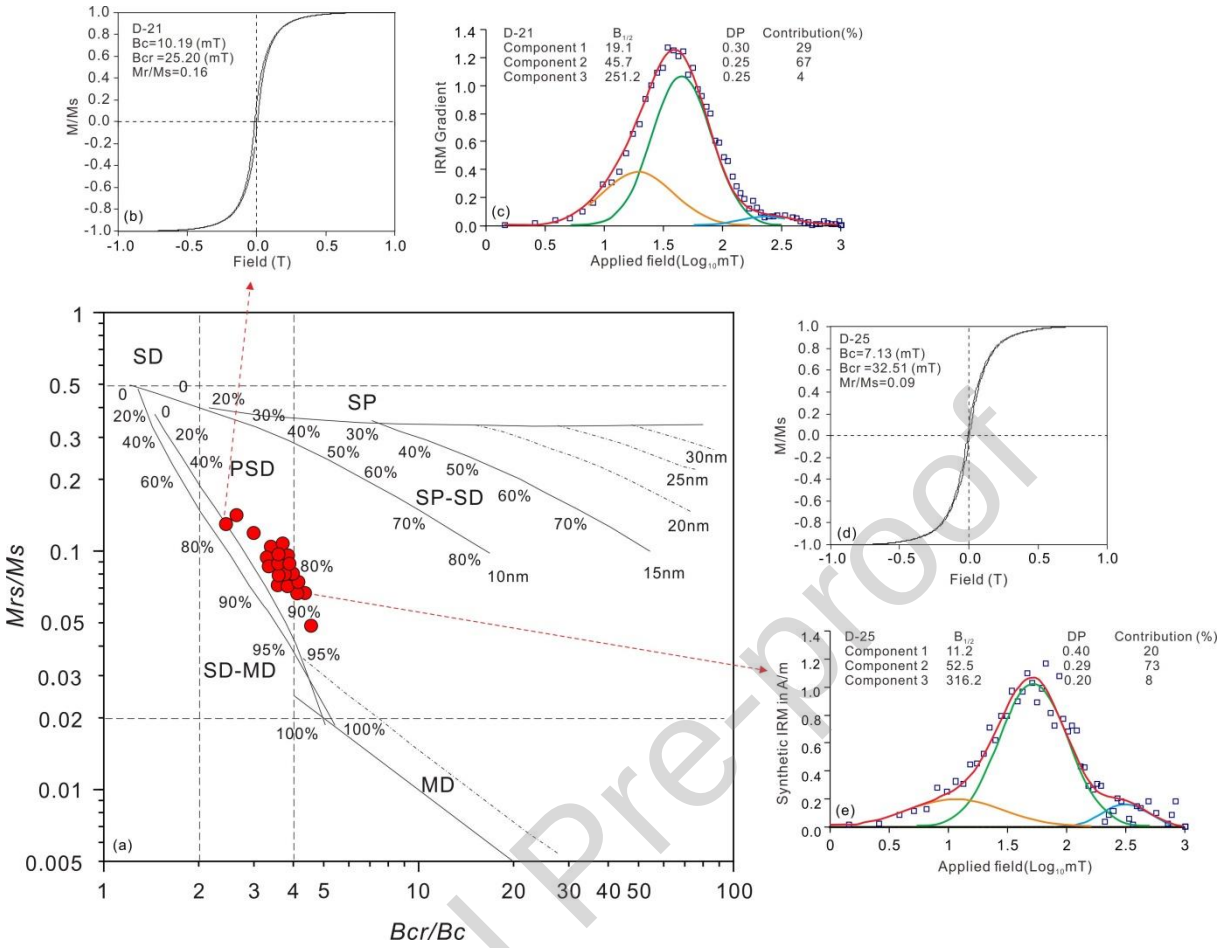

Fig.4 Day plot (a), hysteresis loops (b, d), and IRM gradient curves (c, e) of the two selected samples D-21 and D-25 based on the Day plot.

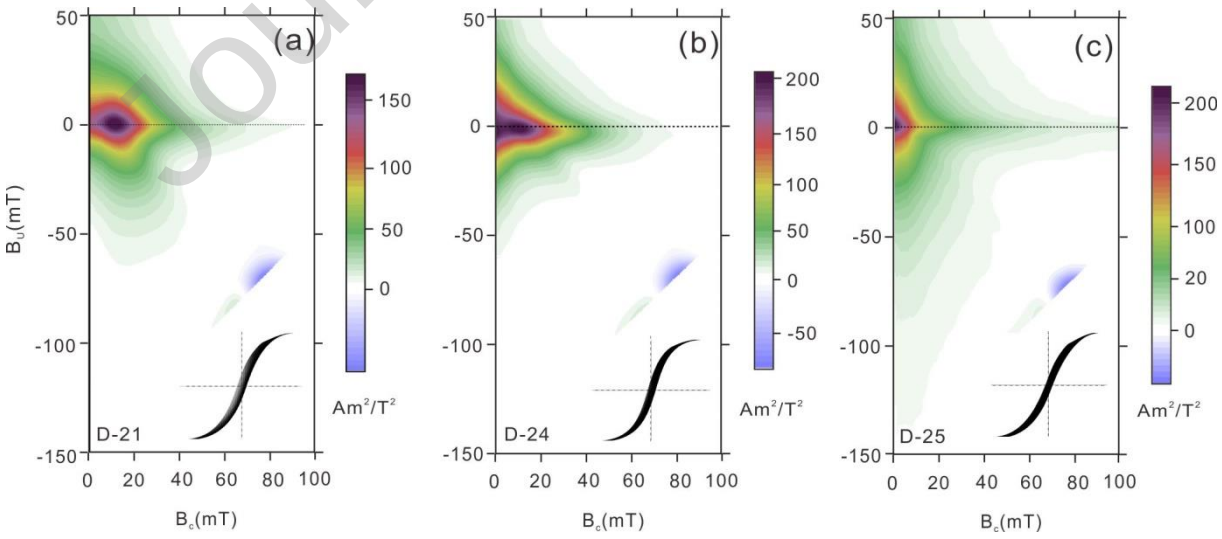

Fig.5 FORC diagrams of the representative household dust samples (a) D-21, (b) D-24 and (c) D-25, which represent mixture of SD and PSD (a-b) and MD (c), respectively. In order to

demonstrate the results of the Day plot, the FORC was also performed on the same two samples D-21 and D-25. Another sample D-24 adjacent to D-21 in the Day plot was also analyzed. VARIFORC parameters used for smoothing the PCA solution are $S_{c,0}$=8, $S_{c,1}$=10, $S_{b,0}$=7, $S_{b,1}$=10, and $\lambda_c=\lambda_b$=0.1.

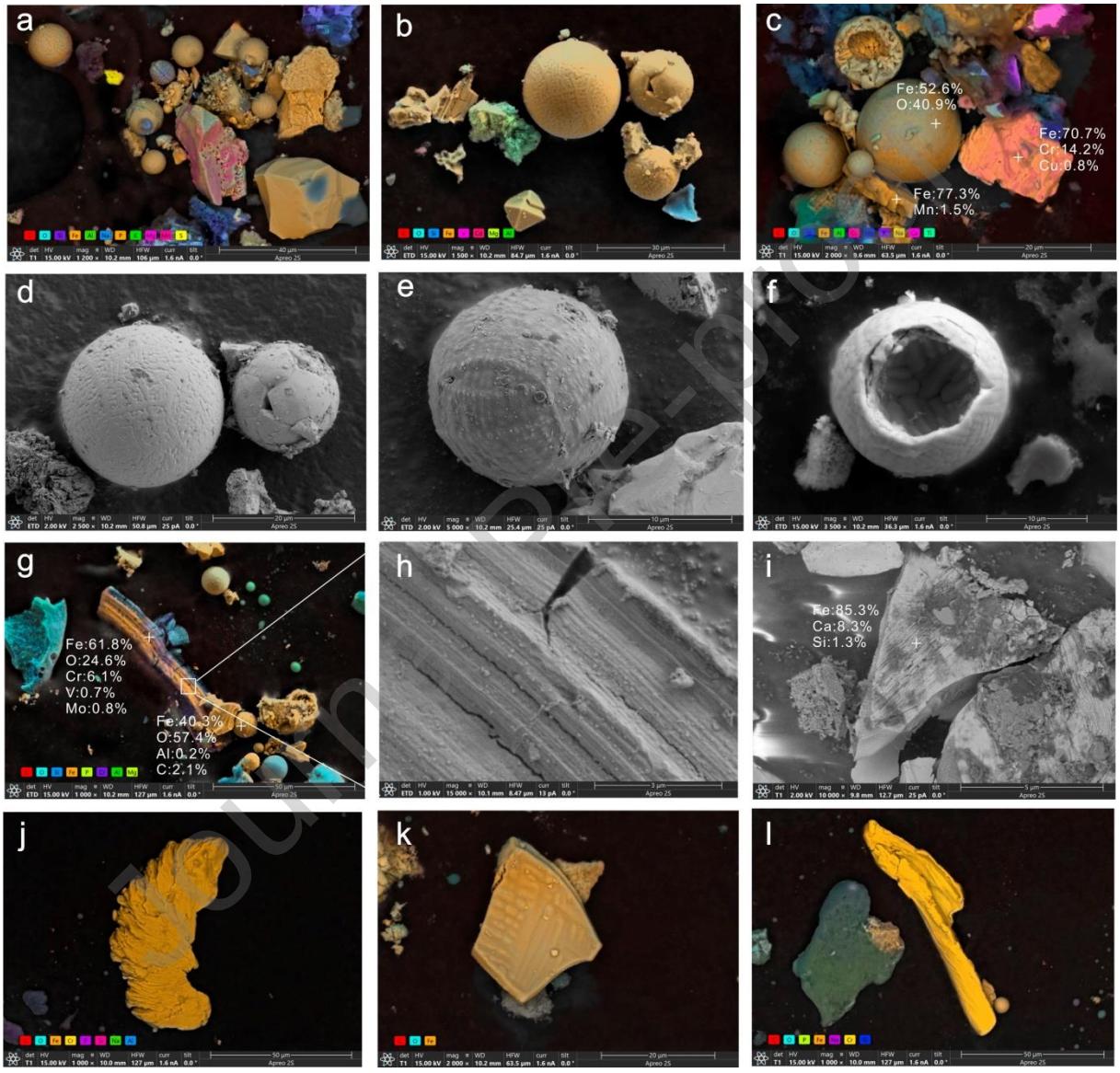

Fig.6 SEM images and element mapping of household dust samples. (a-c) SEM images and element mapping of magnetic extracted samples; (d-f) spherical magnetite particles; (g-i) Scratches on the surface of metallic iron particles likely caused by the braking; (j-l) SEM images of irregular sheet like or blocky iron particles (samples D-2 and D-43).

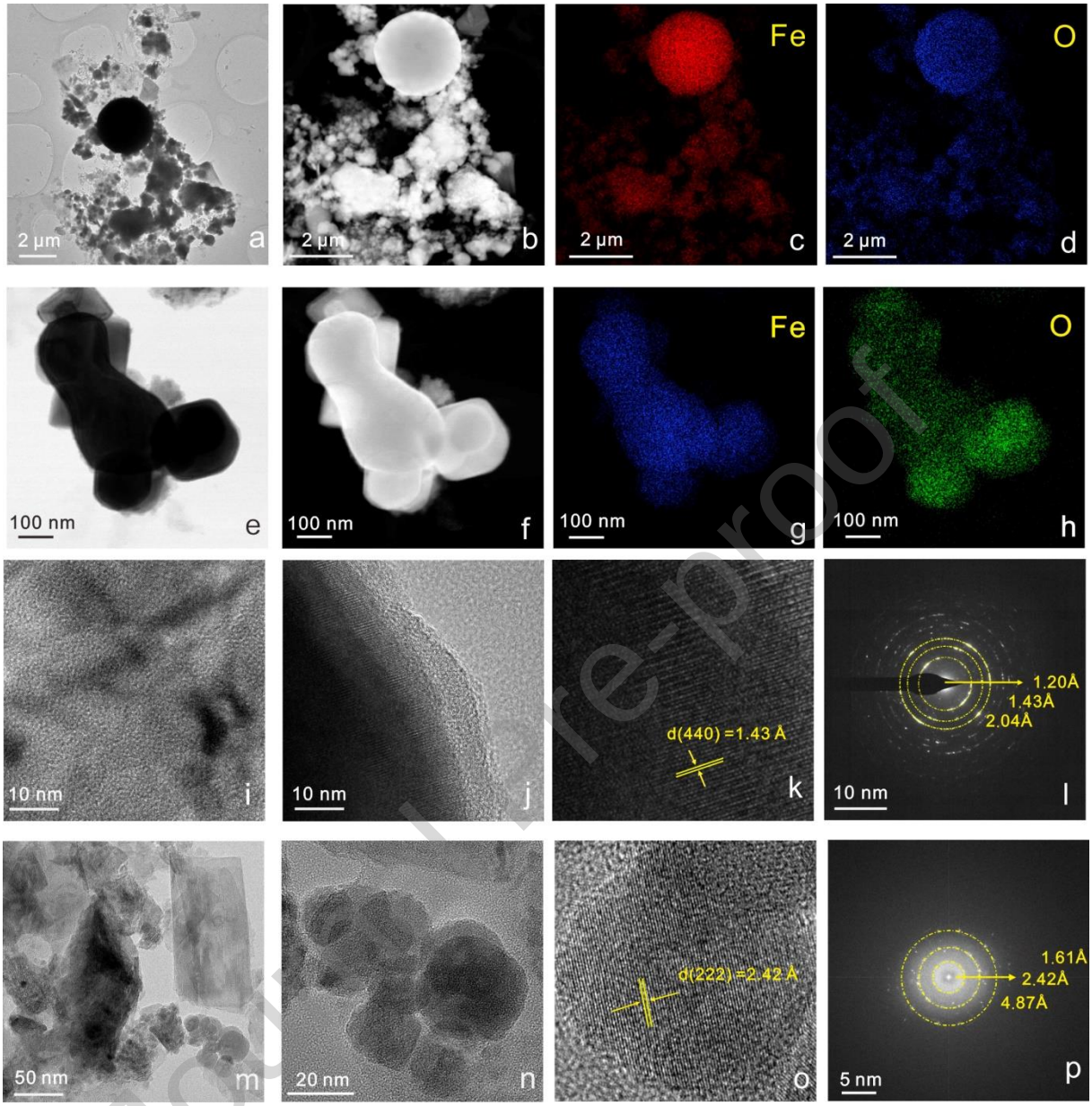

Fig.7 Structural and elemental fingerprinting of household dust in Shanghai. (a,e) TEM image of magnetite; (b, f) HAADF-STEM image of magnetite; (c-d, g-h) EDX mapping of Fe and O for the particles in (b) and (f); (i-k) Atomic resolution HAADF-STEM image of particles in (e); (l) Electron diffraction pattern of particles in (e) with lattice spacing of 1.20, 1.43 and 2.04 Å from inner to exterior, which match the [533], [440] and [400] lattice planes of magnetite; (m-n) TEM image of household dust composed of iron oxide nanocrystals; (o) Atomic resolution HAADF-STEM image of particles in (n); (p) Electron diffraction pattern of particles in (o) with lattice spacing of 1.61, 2.42 and 4.87 Å from inner to exterior, which match the [511], [222] and [111] lattice planes of magnetite.

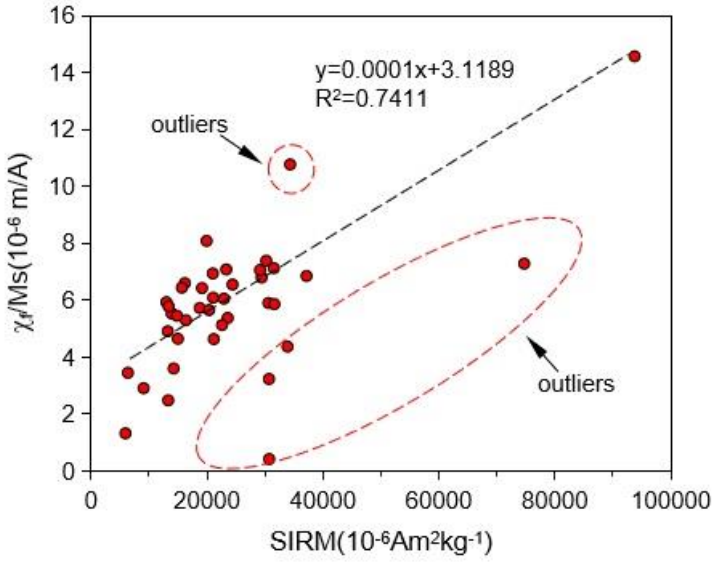

Fig.8 Relationship between saturation isothermal remanent magnetization (SIRM) and normalized ferrimagnetic susceptibility (χ_f/Ms). The outliers as indicated in the plot were excluded from the regression analysis.

Table 1. Magnetic properties of household dusts and its comparison with outdoor dust and soil in Shanghai

Sampling site	χ_{lf} ($10^{-8}m^3kg^{-1}$)	χ_{fd} (%)	χ_{ARM} ($10^{-8}m^3kg^{-1}$)	SIRM ($10^{-6}Am^2kg^{-1}$)	HIRM ($10^{-6}Am^2kg^{-1}$)	S_{-300} (%)	χ_{ARM}/χ	χ_{ARM}/SIRM ($10^{-5}mA^{-1}$)	References
Indoor dust (mean±SD)	187 ± 111	1.7 ± 1.5	408 ± 206	24535 ± 16326	724 ± 503	96.8 ± 2.1	2.3 ± 0.8	17.8 ± 5.6	This study
Indoor dust (median)	178	1.8	391	21075	554	97.4	2.2	17.3	
Indoor dust (25th percentile)	125	0.0	248	14905	367	96.6	1.9	15.7	
Indoor dust (75th	233	2.9	505	30414	948	97.9	2.5	19.7	

percentile)									
Shanghai background soil (mean)	29	2.1	103	2371	344	85.5	3.6	44.0	Hu et al., 2007
Shanghai urban topsoil (mean)	188	2.4	590	26019	879	93.0	3.1	24.0	Wang et al., 2018
Shanghai street dust (mean)	810	2.4	1120	89800	1377	96.5	1.5	13.0	Wang et al., 2019
Dust samples from subway platforms (aboveground) (mean±SD)	1100 ± 320	1.9 ± 1.3	1500 ± 460	140000 ± 48000	3300 ± 2000	97.6 ± 1.6	1.4 ± 0.2	10.9 ± 1.7	Zhang et al., 2011
TSP from industrial zone (mean)	757	5.8	675	112079	6189	95.0	0.9	5.9	Shu et al., 2000

Table 2. Heavy metal(loid)s concentration (mg/kg) of household dust from Shanghai

	Mean (SD) [a]	25th percentile	Median	75th percentile	Range	Shanghai background soil [b]	Maximum/ background soil [c]
As	7.7 ± 4.0	5.4	7.3	10.0	0.2-16.5	7 ± 1	2
Cd	1.7 ± 1.2	0.7	1.2	2.5	0.5-5.1	0.12 ± 0.0	43
Cr	112 ± 42	80	109	131	57-265	88 ± 4	3
Cu	210 ± 115	129	174	252	74-647	28 ± 3	23

Mo	4.3 ± 2.0	3.0	3.7	5.5	1.4-11.7	0.5 ± 0.1	23
Ni	59 ± 24	40	54	70	24-126	37 ± 5	3
Pb	194 ± 128	108	146	252	53-661	27 ± 2	25
Sb	15 ± 8	11	14	19	5-45	0.6 ± 0.1	76
Zn	975 ± 555	645	826	1140	420-3610	107 ± 9	34

[a] Standard deviation in parenthesis.

[b] Values of Shanghai background soil (Cheng et al., 2014).

[c] Maximum values of elements divided by Shanghai background soil values.

Table 3. Comparison of magnetic properties of indoor dust in Shanghai and elsewhere

Sampling site	Description of dust type	χ_{lf} ($10^{-8}m^3kg^{-1}$)	SIRM ($10^{-6}Am^2kg^{-1}$)	Ms (Am^2/kg)	Magnetite concentration (wt %)	χ_{ARM} ($10^{-8}m^3kg^{-1}$)	References
Shanghai, China	Indoor dust, urban areas	186.9	24534.7	0.3	0.3	408.3	This study
	Indoor $PM_{2.5}$ (burning peat)	/	3790	/	0.005-0.006	/	
Ireland	Indoor $PM_{10-2.5}$ (burning peat)	/	3830	/	0.05-0.063	/	Maher et al., 2021
	Indoor $PM_{2.5}$ (burning wood)	/	7780	/	0.01-0.013	/	

	Indoor $PM_{10-2.5}$ (burning wood)	/	6210	/	0.043-0.102	/	
	Indoor $PM_{2.5}$ (burning coal)	/	8920	/	0.12-0.15	/	
	Indoor $PM_{10-2.5}$ (burning coal)	/	19100	/	0.25-0.31	/	
Warsaw, Poland	Indoor dust, heavy traffic areas	163.4	/	0.2011	/	114.3	Górka-Kostrubiec, 2015
	Indoor dust, suburbs	146.1	/	0.1236	/	114.3	
Athens, Greece	Indoor dust, urban areas	181.3	21840	/	/	/	Kelepertzis et al., 2019
Volos, Greece	Indoor dust, heavy industrial areas	244.0	/	/	/	/	Kelepertzis et al., 2021

Credit authorship contribution statement

Yinglu Chen: Methodology, Investigation, Formal analysis, Data curation, Writing – original draft, Visualization. **Weiguo Zhang:** Resources, Writing – review & editing, Funding acquisition. **Chenyin Dong:** Conceptualization, Investigation, Resources, Writing – review & editing, Supervision, Project administration, Funding acquisition. **Simon M. Hutchinson:** Writing- Reviewing and Editing. **Huan Feng:** Writing- Reviewing and Editing.

Declaration of Competing Interest

☒ The authors declare that they have no known competing financial interests or personal relationships that could have appeared to influence the work reported in this paper.

☐The authors declare the following financial interests/personal relationships which may be considered as potential competing interests:

Graphical abstract

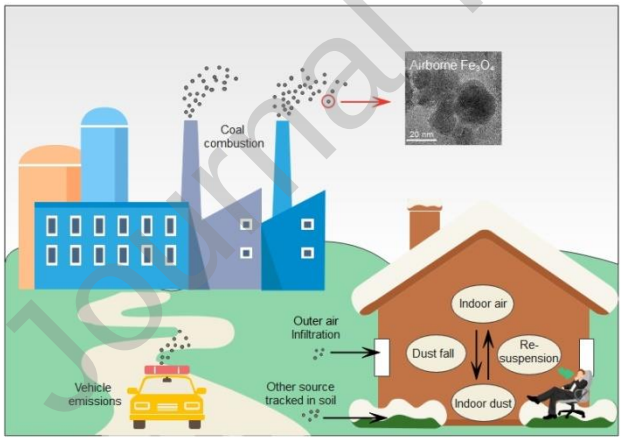

Highlights

- Household dust is characterized by magnetic and geochemical methods and SEM/TEM
- Magnetic particles (IMPs) consist of magnetite, maghemite, hematite and metallic iron
- Nano-sized IMPs increase proportionately with the total IMPs abundance
- IMPs in household dust derive mainly from industrial and traffic emission